JOURNAL OF APPLIED CRYSTALLOGRAPHY

ISSN: 1600-5767
journals.iucr.org/j

Spatially resolved texture analysis of Napoleonic War era copper bolts

Florencia Malamud, Shirley Northover, Jon James, Peter Northover, Stephen Nneji and Joe Kelleher

J. Appl. Cryst. (2017). **50**, 1359–1375

JOURNAL OF APPLIED CRYSTALLOGRAPHY

ISSN 1600-5767

Received 20 January 2017
Accepted 12 August 2017

Edited by A. J. Allen, National Institute of Standards and Technology, Gaithersburg, USA

Keywords: copper bolts; texture; neutron diffraction.

Spatially resolved texture analysis of Napoleonic War era copper bolts

Florencia Malamud,[a]* Shirley Northover,[b] Jon James,[b] Peter Northover,[b,c] Stephen Nneji[b,d] and Joe Kelleher[d]

[a]Laboratorio de Física de Neutrones, Centro Atómico Bariloche, Avenida Bustillo 9500, San Carlos de Bariloche, Rio Negro 8400, Argentina, [b]Materials Engineering, The Open University, Walton Hall, Milton Keynes MK7 6AA, UK, [c]Research Laboratory for Archaeology and the History of Art, South Parks Road, Oxford OX1 3QY, UK, and [d]Rutherford Appleton Laboratory, ISIS Neutron and Muon Source, Harwell, Didcot, Oxford OX11 0QX, UK. *Correspondence e-mail: fmalamud@cab.cnea.gov.ar

The spatial resolution achievable by a time-of-flight neutron strain scanner has been harnessed using a new data analysis methodology (NyRTex) to determine, nondestructively, the spatial variation of crystallographic texture in objects of cultural heritage. Previous studies on the crystallographic texture at the centre of three Napoleonic War era copper bolts, which demonstrated the value of this technique in differentiating between the different production processes of the different types of bolts, were extended to four copper bolts from the wrecks of HMS *Impregnable* (completed 1786), HMS *Amethyst* (1799), HMS *Pomone* (1805) and HMS *Maeander* (1840) along with a cylindrical 'segment' of a further incomplete bolt from HMS *Pomone*. These included bolts with works stamps, allowing comparison with documentary accounts of the manufacturing processes used, and the results demonstrated unequivocally that bolts with a 'Westwood and Collins' patent stamp were made using the Collins rather than the Westwood process. In some bolts there was a pronounced variation in texture across the cross section. In some cases this is consistent with what is known of the types of hot and cold working used, but the results from the latest study might also suggest that, even in the mature phase of this technology, some hand finishing was sometimes necessary. This examination of bolts from a wider range of dates is an important step in increasing our understanding of the introduction and evolution of copper fastenings in Royal Navy warships.

1. Introduction

For several years, neutron diffraction techniques have been used for nondestructive characterization of objects of cultural heritage. This is mainly because thermal neutrons are highly penetrative of most materials and neutron radiation is a versatile diagnostic probe for collecting information from the interior of large museum objects or archaeological finds (Kockelmann, Chapon *et al.*, 2006). In particular neutron diffraction techniques have been used for nondestructive phase analysis of archaeological ceramics and metals (Kockelmann *et al.*, 2001; Kockelmann & Kirfel, 2004; Cartechini *et al.*, 2006; Imberti *et al.*, 2008), residual stress measurements (Santisteban, Siano & Daymond, 2006), and volume texture analyses in ancient copper and copper alloy objects (Artioli, 2007; Siano *et al.*, 2004, 2006; Arletti *et al.*, 2007), Renaissance bronze statuettes (Langh *et al.*, 2011), and 16th-century silver coins (Kockelmann, Chapon *et al.*, 2006). In each case, 'volume texture analysis' means establishing the extent and nature of any preferred orientations among the crystal lattices (Bunge, 1982) of different volumes of a macroscopic sample. There has also been some work using crystallographic texture analysis to

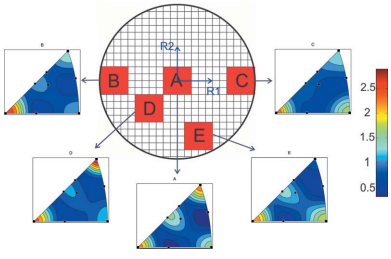

interpret the manufacturing techniques of small archaeological metal artefacts such as prehistoric copper axes (Artioli & Dugnani, 2004), ancient coins (Xie *et al.*, 2004) and Bronze Age axes (Arletti *et al.*, 2008) and to compare the effects of hardening, annealing and recrystallization processes on small standardized specimens with the textures of original archaeological bronze objects directed to the same end (Siano *et al.*, 2004; Kockelmann, Siano *et al.*, 2006).

Crystallographic texture in a polycrystalline material may result from plastic deformation, mechanical working (such as hammering or swaging) or thermal treatments during manufacturing. These working processes each cause distinct preferred grain orientation distributions or textures. Since the crystallographic texture depends strongly on the mechanical deformation and heat treatment processes involved during an object's manufacture, texture analysis and characterization can provide information about the production and deformation history of the sample. Moreover, for archaeological samples, analysis of the texture distributions across a macroscopic sample, using spatially resolved neutron texture analyses, could offer a great advantage for understanding the sample's manufacturing route without involving highly intrusive sampling.

This idea was recently implemented in the data analysis method NyRTex and used to study the crystallographic texture at the centre of three copper bolts from two identified ship wrecks, HMS *Pomone* and HMS *Impregnable* (Malamud *et al.*, 2016). The results demonstrated the value of this technique in distinguishing between the different production processes of the different sizes of bolts without the need for unacceptably intrusive sampling. This was an important step in increasing our understanding of the introduction of copper fastenings into Royal Navy warships. This 'new technology' had become necessary to eliminate the disastrous consequences of the galvanic action between iron fastenings and the copper sheathing applied to wooden warships to protect the timber from attack by *teredo navalis* (shipworm), and as an antifouling measure.

1.1. History of the Navy's use of copper bolts 1760–1830

As soon as HMS *Alarm*, the first ship in the Royal Navy to be sheathed with copper as a protection against the damage caused by shipworm, returned home from a long voyage to the West Indies in 1763 it was apparent that there was a serious problem. Where the copper and iron, two metals of different electrochemical potential, had come into contact in an electrolyte, *i.e.* sea water, the iron was severely corroded. In the structure of the *Alarm* the bolts which secured the timbers and the braces and pintles, the pivots on which the rudder turned, were badly damaged. The next two ships to be experimentally copper sheathed, *Dolphin* and *Tamar*, were sent on a voyage round the world in 1764, the *Dolphin* additionally being fitted with copper braces and pintles while the *Tamar* retained iron. After 18 months, the braces and pintles on the *Dolphin* were well preserved, although the soft metal was rather worn; in contrast, the corrosion of the iron fittings on the *Tamar* nearly caused her rudder to fall off in mid-Atlantic.

The qualified success of the copper braces and pintles on the *Dolphin* led to a proposal in 1768 that a new sloop, about to be laid down at the dockyard at Deptford, be bolted under water with forged copper bolts. This sloop, the *Swallow*, of 14 guns, was launched in 1769 and sailed for the East Indies soon afterwards, where she remained. No problems were reported even when she was re-coppered in Bombay, but no final results were collected because she was lost on the voyage home. Nonetheless, the absence of adverse reports was used to promote, at least for smaller ships, the bolting of new construction with forged copper bolts. This was adopted in early 1777 and the process gradually extended. In 1778 a formal scheme outlining the sizes and locations of bolts for ships of 30 and 50 guns was issued. The contract for their supply was awarded to William Forbes of Primrose Street, Bishopsgate, London, already a contractor for coppersmith's and brazier's wares; Forbes did not have a suitable forge and sub-contracted the work to his copper supplier, George Pengree of Temple Mill, Marlow, on the River Thames.

So far, copper bolting was being applied in new construction of smaller vessels, although by 1782 these could be up to 64 guns, and it was supposed to be restricted to ships built in the Royal Dockyards, where it was believed that tolerances were tighter. It still seems to have been thought that copper bolts did not have the strength necessary for building the largest ships, but a disaster in 1782, when over 2000 lives were lost, concentrated minds and the Admiralty saw that either copper sheathing had to be abandoned or satisfactory copper-based bolts had to be developed. Experiments had been made with copper alloy bolts but the results were found to be unsatisfactory because of a lack of ductility; hindsight has also shown that one of the alloys tested, a copper–iron–zinc composition, had the problem of galvanic corrosion built into it. The solution came in the form of three different patents, taken out in 1783, for cold-rolled copper bolts, with three different approaches to producing cold-hardened copper bolts with a circular cross section.

A Navy Board minute, from late 1783, orders that any iron bolts in the keel of HMS *Impregnable* should be driven out and replaced with copper ones. The wording of the minute suggests the possibility that some copper bolts had already been fitted. Such bolts would have been forged using a swage, a split iron die shaped to give the required circular profile, and a tilt hammer, a heavy hammer operated by a water wheel. At the same time an order was given to Forbes, who was the first to patent cold-rolled bolts with grooved rolls, to produce new copper bolts for the *Impregnable* and these were shipped in November–December 1783. Correspondence from Forbes's brother, who was manager of his rolling mill, informs us as to the realities of the manufacturing process. Copper mainly arrived as ingots weighing from about a half hundredweight to two hundredweight (approximately 25–100 kg) and these had to be reduced to rods of as little as 5/8 inch (16 mm), so there would necessarily be many intermediate anneals (Falkirk Archives A.727.206-2007).

The other two patents were awarded, late in 1783, to John Westwood, for an alternative method of rolling with grooved rolls, and to William Collins, for using the rolls to pull the copper rod through a die. Both Westwood and Collins were associated at this time with Thomas Williams, a lawyer from Anglesey who was gradually building a monopoly position in the British copper market and controlled the massive Parys and Mona mines in Anglesey. Then, in 1784, the Admiralty ordered all new construction to be with copper bolts and all other ships to have their iron bolts replaced – a heroic task which would have been effectively impossible without the use of water-powered rolling mills. In 1785 Forbes gave up his rolling mill, probably because it did not have the capacity to compete with the industrial scale on which Williams was operating. When Williams died in 1802 his successor, Pascoe Grenfell, continued to supply the Navy until, in 1807, the Metal Mill at Portsmouth Dockyard could supply 80% or more of the Navy's requirements, using recycled copper from ships being re-coppered, repaired or broken up. The Metal Mill became so efficient that the Navy did not follow the merchant fleet in using Muntz metal sheathing and fastenings from the 1830s onwards because the copper was cheaper. Over this period, despite copper being as much as ten times the price of iron, copper (and, later, copper alloy) bolts were needed to maintain the protection offered by copper sheathing without the need for repeated re-bolting: a ship might be in service on a foreign station for several years without access to a dockyard, during which time iron bolts would have needed to be replaced more than once. The use of copper in ships was a specialized application which was not generally repeated elsewhere; however, the use of copper fireboxes in British steam locomotives did require the use of arsenical copper stay-bolts suitable for high-temperature service

A number of compositional analyses have shown that all the copper bolts used by the Royal Navy were of the same impure copper which had arsenic, bismuth, lead and silver as the principal impurities, with all the bismuth and much of the lead and arsenic present as oxides (Northover, 2007; Northover & Wilcox, 2013; Northover *et al.*, 2014). The bolts have, at most, 1% arsenic in solid solution, which will have only a modest effect on the yield strength, ductility and recrystallization temperature. The history of the manufacture and use of the bolts shows the possibility of forged, rolled or drawn bolts, worked hot or cold, and with the possibility of a final cold hardening using a swage and tilt hammer. This gives rise to a wide range of possible textures that might be identified, and the potential for texture analysis to differentiate between the different manufacturing systems. The possible variety of textures correlates with the three different textures found in the three bolt sections studied earlier (Malamud *et al.*, 2016). However, two particular questions still unresolved were the extent of the variation in the texture over a cross section and, more broadly, the full range of textures that might be expected. These questions were addressed in the present work by a series of experiments using the time-of-flight neutron diffractometer ENGIN-X. Interpretation of the results included consideration of the possible effects of cold deformation incurred during the driving of the bolts, the working of the ship's hull in service and stresses from the breakup of the wreck.

1.2. Crystallographic conventions

For the benefit of those less familiar with crystallographic conventions and texture measurements, a brief introduction to the representations used for crystallographic information from polycrystalline face-centred cubic (f.c.c.) materials will be included here.

Crystallographic planes and directions are conventionally described by three Miller indices (Randle & Engler, 2000). A direction with vector components **h k l** is represented as [*hkl*] and the set of directions symmetrically related to it by ⟨*hkl*⟩. In a cubic system, a plane with a normal vector **h k l** is represented as (*hkl*) and the set of planes symmetrically related to it by {*hkl*}. Planes and directions are represented in two dimensions using a stereographic projection (Randle & Engler, 2000). Owing to the high symmetry of f.c.c. materials such as copper, all possible orientations in space can be represented within the area of the stereographic projection bounded by [001], [101] and [111]. (Those unfamiliar with the use of Miller indices may find it useful to remember that in f.c.c. materials the {111} planes are the close-packed planes, the ⟨110⟩ directions are the close-packed directions, and ⟨001⟩ are the *x*, *y* and *z* axes of the cubic structure.) The strength of a preferred orientation along any direction is measured by comparing the number of crystallites (or the volume of material) of that orientation along the direction of interest with that from a completely untextured material. This is expressed in multiples of a random distribution (m.r.d.)

1.3. Metal working and texture

Different metal-working processes such as hammering, rolling, or drawing and annealing can lead to alignment of distinctive crystallographic planes or directions, causing what is known as texture. A comprehensive treatment of this subject is given by Kocks *et al.* (2004) and a simple description of how this arises will be presented here to facilitate the more specific discussion later in this paper. Working f.c.c. metals usually produces plastic deformation by generating and moving dislocations, and this changes the local orientation of the metal crystals. Dislocations in metals generally move more easily on close-packed planes and in close-packed directions and, as deformation proceeds, grain orientations change so that such favoured planes and directions are closer to the direction of the main applied stresses. During hammering and rolling of a metal, the constraints on the metal's shape, while it is deforming, are different in each case, so the two processes produce different textures. In general, ⟨110⟩ tend to align along the direction of compression and ⟨111⟩ tend to align along the tensile direction. Annealing, which recrystallizes the structure, does not completely randomize the metal's texture but leads to complex textures retaining and modifying some elements of the deformation texture. In describing texture, its

components are referred to by the planes and directions that are preferentially aligned. For example, rolling copper may produce a $\{110\}\langle 1\bar{1}2\rangle$ and/or $\{123\}\langle 1\bar{2}1\rangle$ texture (Taylor, 1961). Drawing a wire produces what is known as a fibre texture in which one specific set of directions is aligned (frequently along the drawing axis), and the texture is described simply by the Miller indices of that preferred direction. Drawing copper frequently produces a double-fibre texture in which both $\langle 111\rangle$ and $\langle 001\rangle$ are preferentially aligned (Taylor, 1961).

2. The analysed bolts

The present spatially resolved texture analysis investigation involves copper bolts from four identified wrecks, HMS *Impregnable*, HMS *Amethyst*, HMS *Pomone* and HMS *Maeander*. These four ships represent important phases in the history described above and will be presented in chronological order:

HMS *Impregnable*, a 'second rate' 90-gun ship of the line of the London class, was laid down at HM Dockyard, Deptford, in October 1780. In late 1783 it was ordered that where possible any iron bolts should be driven out and replaced with copper; copper bolts were ordered from William Forbes in November 1783 and the bolt studied here has a Forbes stamp. The *Impregnable* was completed in May 1786, had some repairs in 1794 and was lost in 1799.

HMS *Amethyst* was a 'fifth rate' with 36 guns of the Penelope class, ordered in 1797 and completed in 1799. She was wrecked at Plymouth in 1811. The excavation of the wreck has produced a variety of bolts, including one with a Westwood and Collins patent stamp and one with a Forbes stamp. The latter needs explanation because the *Amethyst* was ordered 14 years after Forbes had given up his rolling mill; most probably the bolt was reused from another ship.

HMS *Pomone*, a 'fifth rate' 38-gun frigate of the Leda class, was laid down at Brindley's Yard on the Medway at Frindsbury in December 1803 and completed on 17 January 1805. No subsequent repairs are documented so the bolts recovered from her wreck will be original. She represents the full maturity of the production of copper bolts by private industry before they were largely superseded by the Metal Mill at Portsmouth Dockyard.

HMS *Maeander* was a 'fifth rate' with 48 guns, a modified Leda class vessel ordered in 1824. Her keel was laid in 1829, at Chatham, but she was not finally completed until 1840, entering service in 1847. Ultimately, she was sent to Ascension Island and paid off there in 1866. The stripped hull was wrecked in 1870. For this study, the *Maeander* represents the copper bolts produced at Portsmouth Dockyard.

Table 1 gives details of the bolts' diameters.

Table 1
Sizes of the bolts studied.

Ship	Completed	Lost	Bolt length (mm)	Bolt diameter (mm)
HMS *Impregnable*	1786	1799	956.0	35.5
HMS *Amethyst*	1799	1811	631.0	41.0
HMS *Pomone* (segment)	1805	1811	–	33.5
HMS *Pomone* (AB1-02-01)	1805	1811	330.0	22.5
HMS *Maeander*	1840	1866	686.0	35.5

3. Spatially resolved neutron texture analysis

The main goal of texture experiments is to obtain the orientation distribution function (ODF), which gives a complete description of the crystallographic texture of the sample. The ODF can be defined from least-squares fits to a number of experimentally derived incomplete pole figures. These are measured by collecting neutron diffraction patterns from many different angles, either by rotating the sample or by using a detector with a large angular coverage around the specimen. In time-of-flight neutron diffractometers such as the General Materials Diffractometer (Williams *et al.*, 1997) at ISIS in the UK or the High-Pressure Preferred Orientation Diffractometer (Matthies *et al.*, 2005) at Los Alamos in the USA, with a large number of detectors around the sample position, no sample rotation is required, and the texture of a bulky object can be analysed in one measurement. However, the low spatial resolution of these instruments precludes studies of the spatial variation of the texture across macroscopic specimens, since this requires measurements localized on a specific region of the object. Such measurements could, however, be done in the time-of-flight neutron diffractometer engineering materials beamline.

ENGIN-X (Santisteban, Daymond *et al.*, 2006) at ISIS in the UK is optimized to measure elastic strains at precise locations in bulky specimens. ENGIN-X has only two diffraction banks perpendicular to the incident beam, each covering a $30 \times 30^{\circ}$ solid angle around the sample, and a two-dimensional transmission bank. The volume of material contributing to each diffraction pattern, the gauge volume, corresponds to the intersection of the incident and diffracted beams, usually defined by slits and collimators, respectively, and is typically of the order of cubic millimetres. The centroid of this gauge volume defines the measurement location. Since the gauge volume is at a fixed position in the laboratory, the texture variation across the sample can be explored by moving the sample using a goniometer or a translation stage. Typical diffractograms, for different locations [A, B, C, D and E in Fig. 1(*b*)] across the HMS *Pomone* copper bolt cross section, are shown in Fig. 1(*c*). In standard strain scanning experiments, all neutrons arriving at a detection bank are combined into a single diffractogram by a post-analysis routine, as is shown in Fig. 1(*c*). The diffractograms have been recorded by the North bank with the sample oriented as shown in Fig. 1(*a*), *i.e.* each diffraction peak *hkl* provides information about the number of crystallites having their (*hkl*) plane normals centred around the bolt axis direction (BA). As is observed in the figure, the 111 and 200 peak intensities decrease from the centre to the bolt surface, suggesting a texture gradient across the bolt diameter. However, in ENGIN-X, a series of measurements in different sample orientations are needed to define an incomplete pole figure for each location. Since two specimen directions are measured simultaneously by the

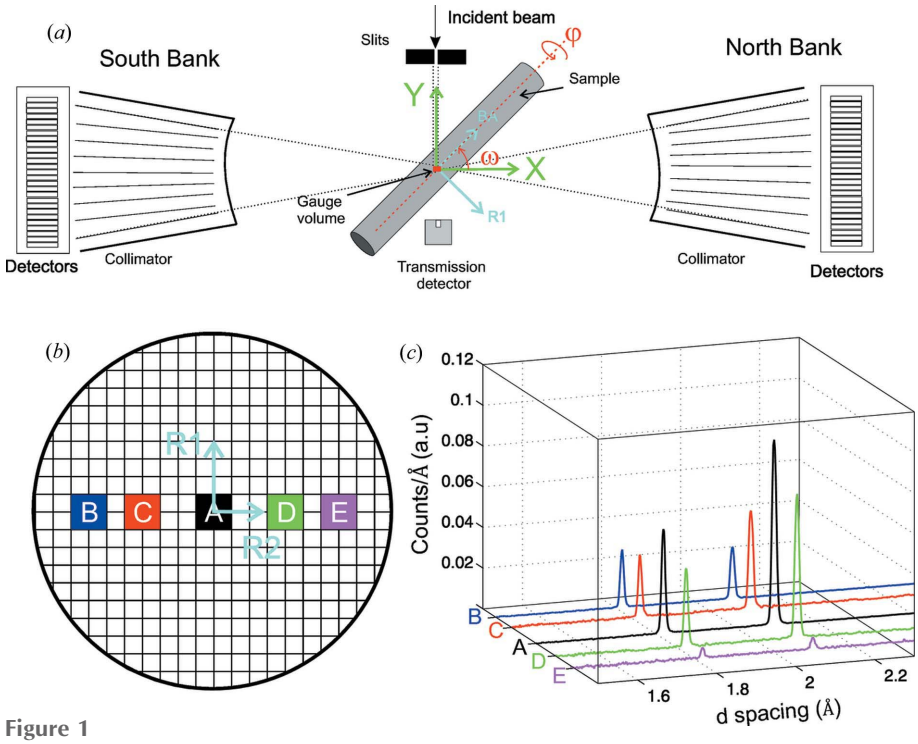

Figure 1
(*a*) Schematic diagram of the ENGIN-X time-of-flight neutron strain scanner, with a bolt at the sample position. (*b*) Explored locations on the HMS *Pomone* bolt cross section (grid spacing 1 mm). (*c*) Diffactograms collected in the bolt axis direction from different locations across the bolt diameter.

instrument, the full coverage of the orientation space using a $5 \times 5^\circ$ grid would require 648 orientations, a prohibitively large number when considering the necessary measurement time and very high demand for such instruments. With the aim of minimizing the number of orientations required to define a pole figure, and to obtain a better angular resolution, we have recently proposed a new data analysis methodology, NyRTex (Malamud *et al.*, 2014), which involves regrouping the individual detectors composing the diffraction banks into smaller groups of higher angular resolution. The method is based on the determination of several incomplete pole figures after splitting the detector arrays into several units of smaller angular coverage. Determination of the ODF of the crystallites from the incomplete pole figures is accomplished by means of *MTEX* (Hielscher & Schaeben, 2008), a texture analysis library based on an algorithm especially suited for sharp textures and high-resolution pole figures measured on scattered specimen directions. A complete description of the NyRTex data analysis methodology is given by Malamud *et al.* (2014) so only a brief description is provided here.

3.1. Texture analysis methodology

The data analysis scheme implemented in NyRTex involves subdividing the large solid angle subtended by each detector bank into several virtual detectors with smaller angular coverage, by regrouping the 1200 elements composing each ENGIN-X bank. This is done by time-focusing all the neutrons arriving at all the detection elements of each new virtual detector into a single diffractogram. For a fixed position of the sample, the virtual detector's location in the pole figure is determined by the transformation matrix between the laboratory reference system [green *XYZ* coordinate system in Fig. 1(*a*)] and the sample reference frame. This matrix is defined by the coordinates of the sample's principal directions in the fixed laboratory reference system. To explore the pole figure, the sample is usually rotated by an automated mechanical device such as a translation stage or a goniometer. At ENGIN-X a choice of different goniometers is available to achieve this, depending on the size and weight of the specimen being investigated. In each case, the principal coordinates are expressed as the direction cosines for each orientation system in the laboratory reference frame. In this way, it is possible to incorporate the orientation as a function of the rotation angles of the device (χ, ω, φ) and for a chosen detector array, and NyRTex determines the corresponding virtual detector position in the pole figure for each orientation. The number of virtual detectors used in each experiment emerged as a compromise between the desired angular resolution and the statistical uncertainty of the experiment.

Construction of the experimental pole figure $P_{hkl}(\alpha, \beta)$ (α being the latitude angle and β the longitude) requires a quantitative determination of the integrated peak area recorded by a virtual detector along a certain direction of the specimen. In NyRTex the integrated areas (I_{hkl}) of selected peaks of the diffractograms are obtained by least-squares fitting to the experimental data, using a multi-peak fitting algorithm based on asymmetric peak profiles [each the convolution of a Gaussian with a truncated exponential (Kropff *et al.*, 1982)] superimposed on a linear background. However, to produce a combined pole figure from data registered by different virtual detectors, several corrections need to be applied to the refined peak area measured by each individual virtual detector. In addition to the texture factor, the integrated intensity of a diffraction peak measured in a time-of-flight (TOF) diffractometer depends on the scattering power (G_{hkl}) and linear absorption coefficient (μ_{hkl}) of the sample, as well as on an instrumental factor ($\Phi^j_{\rm inst}$) specific to each virtual detector (j). Hence, the pole figure intensity (P_{hkl}) recorded by a virtual detector is obtained from the measured integrated peak area according to

$$P_{hkl}(\alpha, \beta) = I_{hkl}(\alpha, \beta)/[G_{hkl} \exp(-l\mu_{hkl})\Phi^j_{\rm inst}], \qquad (1)$$

l being the length of the neutron path inside the specimen.

The scattering power is given by $G_{hkl} = m_{hkl}|F^2_{hkl}|d^4_{hkl}/v_0{}^2$, where v_0 is the volume per atom, F^2_{hkl} the structure factor (including the Debye–Waller factor), m_{hkl} the multiplicity of the reflection and d_{hkl} the interplanar distance of the reflection. The instrumental factor for each virtual detector depends both on geometrical aspects, such as the mean Bragg angle, the distance to the sample and the virtual detector height, and on instrumental parameters, such as the gauge volume, the incident neutron flux $\Phi^j_0(\lambda)$, the detection efficiency $\varepsilon_j(\lambda)$ and the divergence of the incident beam. However, in general the wavelength dependence of $\Phi^j_{\rm inst}$, contained in the product term $\Phi^j_0(\lambda)\varepsilon_j(\lambda)$, is usually approximated by measuring the spectra scattered by a $V_{0.97}Nb_{0.3}$ sample under the same experimental conditions.

Since a diffraction peak measured on a TOF diffraction bank contains contributions from neutrons with a range of wavelengths, from $\lambda_{\rm min} = 2d_{hkl}\sin\theta_{\rm min}$ to $\lambda_{\rm max} = 2d_{hkl}\sin\theta_{\rm max}$, where $\theta_{\rm min}$ and $\theta_{\rm max}$ are the minimum and maximum Bragg angles of neutrons incident on the detector bank, the attenuation coefficient μ_{hkl} for a particular reflection can be calculated by averaging the total cross section over the associated wavelength range (Wang *et al.*, 2001):

$$\mu_{hkl} = \frac{N\int_{\lambda_{\rm min}}^{\lambda_{\rm max}} \sigma_{\rm tot}(\lambda)\,{\rm d}\lambda}{\lambda_{\rm max} - \lambda_{\rm min}}. \qquad (2)$$

3.2. Sample positioning and neutron path length calculation

To investigate the texture along different specimen directions, the samples were placed in a Cybaman manipulator, a three-axis goniometer supporting specimens of up to 20 kg, fixed to a three-axis positioning table (Fig. 2*a*). After precise alignment of the specimen, the region to be investigated was brought to the centre of the diffractometer by translations with the positioning table and the TOF diffractograms were collected in several sample orientations. The convention adopted for the sample and laboratory reference systems is detailed in Fig. 1(*a*). The (green) *XYZ* coordinate system is attached to the sample, the *X* axis pointing to the centre of the North detection bank, the *Y* axis pointing to the incident beam direction and *Z* along the vertical. The (blue) $x'y'z'$ coordinate system is attached to the centre of the sample, which for a bolt would correspond to the bolt axis direction, and two perpendicular radial directions (R1 and R2), arbitrarily defined. In the laboratory reference system, each sample orientation is defined by the angles (χ, ω, φ), where χ allows the bolt axis to tilt anticlockwise from the vertical axis (rotation around the *Y* axis); ω allows the sample to rotate clockwise around the *Z* direction and φ represents the anticlockwise rotation axis around the sample holder, *i.e.* the bolt axis direction. The sample and laboratory systems coincide for $\chi = 0°$, $\omega = 0°$, $\varphi = 0°$, as is shown in Fig. 2(*a*) for the HMS *Impregnable* copper bolt. In this orientation, the R1 direction points along *X*, the R2 direction along *Y* and the bolt axis direction along *Z*. The sample orientation in Fig. 1(*a*) corresponds to an orientation characterized by $\chi = 90°$, $\omega = -45°$, $\varphi = 0°$.

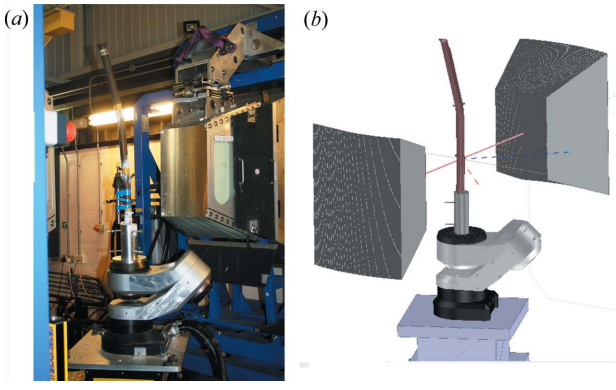

Figure 2
(*a*) Experimental setup for the HMS *Impregnable* copper bolt using the Cybaman goniometer for $\chi = 0°$, $\omega = 0°$, $\varphi = 0°$. (*b*) Screen capture of the corresponding *SScanSS* simulation, including the calibrated sample positioning system, laser scanned sample model and ENGIN-X detector banks.

Data collection for this experiment required measurement points to be accurately positioned at the centre of the instrument gauge volume while simultaneously controlling the orientation of the samples around the three independent axes [(χ, ω, φ) angles]. These requirements, coupled with the considerable length of some of the bolt samples, their irregular geometry, and the constrained working space defined by the jaws and collimators of the ENGIN-X instrument, necessitated use of new positioning methodologies recently developed for the ENGIN-X instrument (Nneji *et al.*, 2016). Based on techniques from robot calibration, these methods rely on the construction of a highly accurate kinematic model of the combined table and goniometer. This model is then used within the existing *SScanSS* virtual laboratory control software (James *et al.*, 2004) to provide both a simulation of the experiment and accurate automated instrument control. The virtual sample models allow both the measurement points and the required orientations to be specified in the sample coordinates, and knowledge of the disposition of the sample and the instrument for each measurement allows the various neutron path lengths, as required by equation (1), to be calculated automatically. The experimental setup and corresponding *SScanSS* virtual model for the HMS *Impregnable* copper bolt at $\chi = 0°$, $\omega = 0°$, $\varphi = 0°$ are shown in Figs. 2(*a*) and 2(*b*), respectively.

4. Results and interpretation

4.1. HMS *Impregnable*

The complete bolt studied here, IMP-006 in the excavation archive, is 956 mm long and 35.5 mm in diameter, probably joined major timbers in the fore part of the ship, and is almost certainly original to her construction. The diameter is the same as that of a batch of boltstaves (lengths of copper rod from which bolts were cut at the dockyard) which was supplied to Deptford in November 1783 and one of the first produced in

Forbes's rolling mill. The bolt is one of very few with a Forbes works stamp, as is shown in the inset in Fig. 3(*a*).

The complete bolt central point texture was studied using ENGIN-X and the full ODF reconstructed from the experimental data using NyRTex (Malamud *et al.*, 2016). The data were analysed in a 2 × 5 (horizontal × vertical) gridding scheme, which gives each virtual detector a coverage of ∼8 × 8° in angular space. The recalculated pole figures display a weak texture, with maximum and minimum pole densities of about 2.4 and 0.2 m.r.d., respectively. {001}⟨100⟩, {122}⟨212⟩, {111}⟨2$\bar{3}$1⟩ and {111}⟨$\bar{1}\bar{1}$2⟩ are the main texture components present in the ODF section plots. The absence of a more significant texture might seem to indicate that the bolt has been neither strongly worked nor extensively heat treated (Arletti *et al.*, 2007). However, the copper is known to have been reduced from a billet to a bar and then reduced to its present size either by grooved rolls or through a swage (W. Forbes, 1783; D. Forbes, 1783). The {001}⟨100⟩ and {122}⟨212⟩ components are typical cube and twin cube components resulting from recrystallization during thermal annealing of rolled f.c.c. metals. Their presence is taken as evidence of thermal treatment after mechanical working, because oriented recrystallization cannot take place unless the crystallites have previously been rotated by plastic deformation (Artioli, 2007). On the other hand, the presence of the {111}⟨2$\bar{3}$1⟩ and {111}⟨$\bar{1}\bar{1}$2⟩ components demonstrates that the sample is not completely annealed, since it retains texture features related to mechanical working in the bolt axis direction.

To explore texture variations across the bolts, neutron texture measurements were performed for the complete bolt from HMS *Impregnable*, defining incomplete experimental pole figures at different locations across its cross section (Fig. 3*b*): at the bolt centre (position A), close to the surface

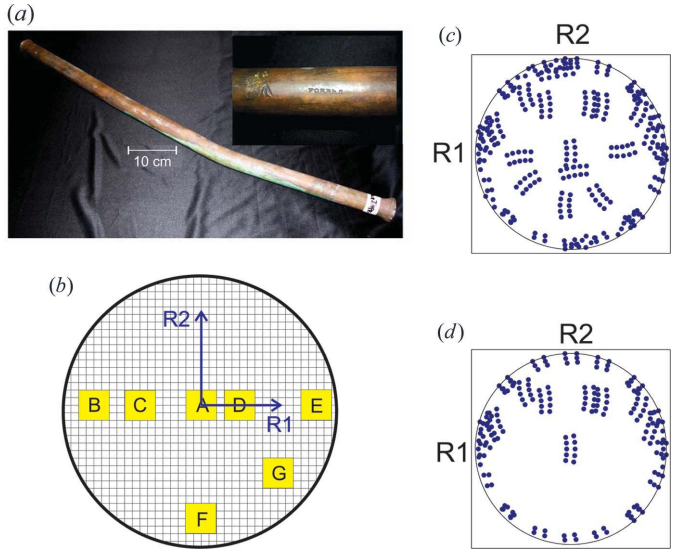

Figure 3
(*a*) HMS *Impregnable* bolt with a Forbes works stamp. (*b*) Explored positions across the bolt cross section (grid spacing 1 mm). (*c*) Stereogram showing the expected pole figure coverage achieved by the chosen texture strategy for point A. (*d*) Expected pole figure coverage for other positions across the bolt cross section.

Table 2
Measurement positions in the Forbes bolt and the number of virtual detectors used for each experimental pole figure.

	Coordinates (mm)			Virtual detectors with $\exp(-l\mu_{hkl}) > 0.01$			
	R1	R2	Measured orientations	{111}	{200}	{220}	{311}
A	0	0	16	272	269	260	279
B	−14.5	0	10	168	167	165	169
C	−8	0	10	167	174	166	174
D	5	0	10	173	175	170	178
E	14.5	0	10	178	174	173	178
F	0	−14.5	10	171	171	167	171
G	10	−10	10	172	171	171	169

(positions B, E, G and F), and between the centre and the outer zone (positions C and D). Following the cylindrical symmetry of the samples, a macroscopic coordinate system, centred at point A, was defined by the BA and two perpendicular radial directions (R1 and R2), arbitrarily defined. The explored positions in this sample coordinate system are shown in Table 2.

For each point, neutron experiments were performed using an incident beam divergence of ∼0.7 × 0.8° (horizontal × vertical). Sequentially, the bolt axis was placed vertically ($\chi = 0$), as shown in Fig. 2(*a*), horizontally ($\chi = 90°$), and tilted to 30 and 45° from the vertical. Owing to the sample's cylindrical shape, the experiments were performed using a 10 × 4 × 4 mm gauge volume in the vertical configuration and a 4 × 4 × 4 mm gauge volume in the other cases. For each bolt axis configuration, several measurements were performed, rotating the sample around the vertical instrument axis (varying ω) and around the bolt axis direction (varying φ). TOF diffractograms were recorded at 16 specimen orientations for position A, and at ten orientations for the other positions, with counting times of ∼12 min per orientation.

The data were analysed in a 2 × 5 (horizontal × vertical) gridding scheme, giving each virtual detector a coverage of ∼8 × 8° in angular space. A single diffractogram was compiled for each virtual detector, by adding together the TOF spectra recorded by all the individual detector elements belonging to that group using a common *d*-spacing scale. This strategy yielded, for each experimental pole figure, a total of 320 virtual detectors for point A (Fig. 3*c*) and a total of 200 virtual detectors for positions B, C, D, E, F and G (Fig. 3*d*). However, because of the Forbes bolt's large diameter, the path lengths for some virtual detectors generated extremely low absorption correction factors for some reflections. To include only the useful detectors, the {111}, {200}, {220} and {311} experimental pole figures for each point were generated using the integrated intensities and the respective correction factors only for the virtual detectors with $\exp(-l\mu_{hkl}) > 0.01$. In some positions across the bolt diameter this considerably reduced the number of contributing virtual detectors for different reflections, as is shown in Table 2. Nevertheless, with this number of virtual detectors it is still possible to calculate with *MTEX* the ODF for each point from the {111}, {200}, {220} and {311} experimental pole figures assuming triclinic sample symmetry.

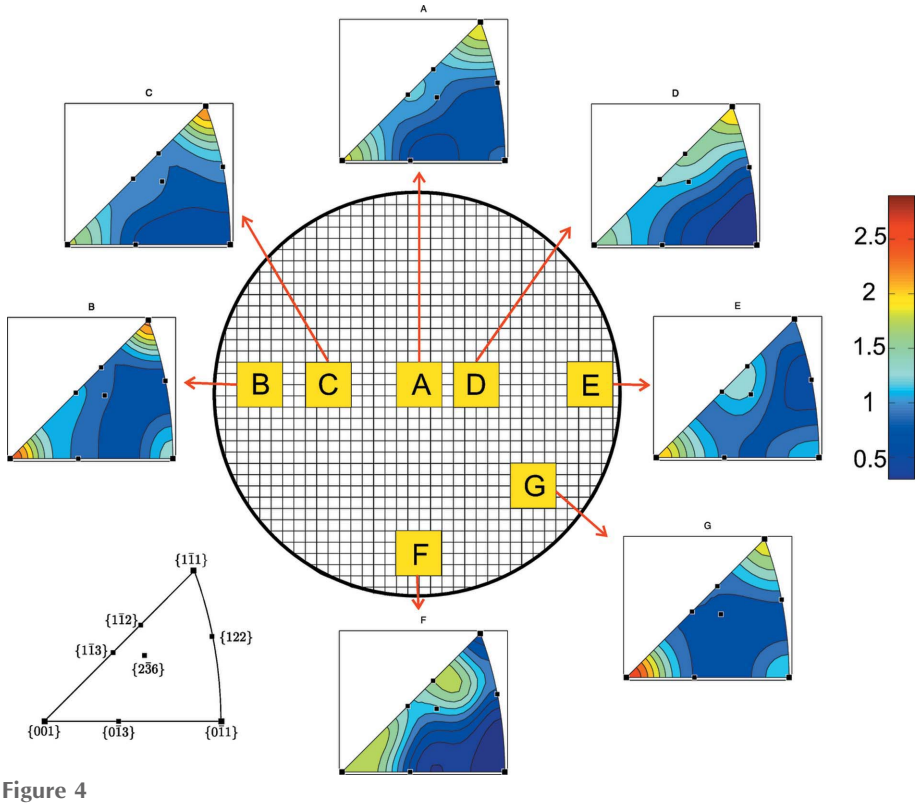

Figure 4
Inverse pole figures from each measurement volume in the Forbes bolt (grid spacing 1 mm). All use the same colour scale in m.r.d.

The texture results for each point across the sample cross section are presented as the inverse pole figures (IPFs) in the bolt axis direction. The inverse pole figure can be defined in the crystal coordinate system as the probability that a sample direction is parallel to an arbitrary crystal direction [*hkl*] and may be thought of as the two-dimensional projection of the orientation density in the crystal space. Similarly to the direct pole figure, the colour scale represents pole densities in units of m.r.d. The recalculated IPFs for each position, looking along the bolt axis, are shown, using the same colour scale, in Fig. 4, together with the standard reference cubic crystallographic triangle. The principal texture features are similar in all positions across the bolt diameter (B, C, A, D and E), with intense {111} and {100} type components and smaller {122}, {112} and {4 4 11} type components parallel to the bolt axis direction. In particular, the {001}⟨100⟩ component and the {122}⟨212⟩ component result from recrystallization during thermal annealing of rolled f.c.c. metals, and the {111}⟨2$\bar{3}$1⟩ and the {111}⟨$\bar{1}\bar{1}$2⟩ components are related to mechanical working in the bolt axis direction. These components are the same as those discussed earlier. However, a closer analysis shows the presence of a smaller {112}⟨$\bar{1}\bar{1}$1⟩ copper type component and a {4 4 11}⟨11 11 $\bar{8}$⟩ Taylor type component, which are typical deformation textures in f.c.c. metals (Kocks *et al.*, 2000).

Fig. 5(*a*) shows the volume fractions of the main texture components at different positions across the bolt diameter, as a function of the distance from the centre. The volume fractions were computed using *MTEX* with a 15° radius sphere centred at each orientation. The volume fraction of the {001}⟨100⟩ component decreases almost linearly from the surface to the centre of the sample, while the {111}⟨2$\bar{3}$1⟩ and {111}⟨$\bar{1}\bar{1}$2⟩ volume fractions show the opposite behaviour, with higher volume fractions towards the centre of the bolt. The presence

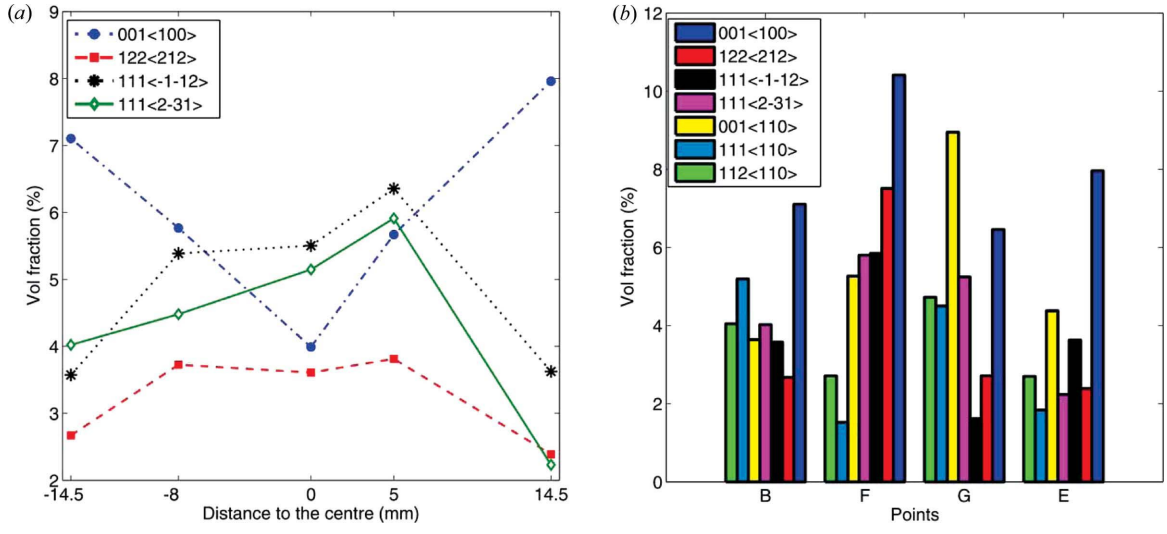

Figure 5
HMS *Impregnable* bolt. (*a*) Principal texture component volume fractions as a function of the distance from the bolt centre. (*b*) Volume fractions for points close to the bolt surface.

of the {001}⟨100⟩ and {122}⟨212⟩ components is taken as evidence of thermal treatment after mechanical working, as the orientated recrystallization cannot take place without previous rotation of the crystallites due to plastic deformation (Artioli, 2007). However, the bolt showed incomplete recrystallization during thermal annealing, since the centre of the sample still preserves texture components related to mechanical working in the bolt axis direction. Similar behaviour was observed in prehistoric copper axes where the presence of some textural features related to mechanical working in one or two directions has been associated with incomplete thermal recrystallization (Artioli, 2007).

On the other hand, the IPFs from the points B, E, F and G which are closer to the bolt surface show more shear type texture components, such as {001}⟨110⟩, {111}⟨110⟩ and {112}⟨110⟩. Fig. 5(*b*) shows, for each point close to the bolt surface, the volume fractions of the main texture components and the shear texture components, as computed by *MTEX* using a 15° radius sphere centred at each orientation. As is shown in the figure, the cube component due to recrystallization is the principal texture component at all points close to the bolt surface. The presence of the shear components could be understood as part of an ideal 'B partial fibre' {*hkl*}⟨110⟩ (Kocks *et al.*, 2000), because the ⟨110⟩ directions are the principal directions in the uniaxial deformation mode in f.c.c. metals. Those components could be associated with torsional deformation, resulting from the documented cold hardening of the surface of the bolt, from the driving of the bolt into the hull and its subsequent mechanical history in a continually flexing hull, or, possibly, from stresses during the breakup of the wreck on the sea bed.

4.2. HMS *Amethyst*

This bolt was selected because it had a Westwood and Collins patent stamp, the first so identified to be studied, and one aim was to use the texture analysis to determine whether Westwood's or Collins's process had been used to produce it.

The crystallographic texture at the centre of the HMS *Amethyst* bolt (Fig. 6*a*) was measured using an instrument configuration and data analysis strategy identical to that used for the HMS *Impregnable* sample. TOF diffractograms were collected at 14 specimen orientations with counting times of ∼12 min per orientation, using a 4 × 4 × 4 mm gauge volume. The {111}, {200}, {220} and {311} experimental pole figures were generated from the integrated intensities and the respective correction factors for those virtual detectors with $\exp(-l\mu_{hkl}) > 0.01$. The pole figure coverage obtained by this strategy is shown in Fig. 6(*b*) for the {111} experimental pole figure. Again, the ODF of the material was calculated with *MTEX* from the experimental pole figures, assuming triclinic sample symmetry. The recalculated pole figures of Fig. 6(*c*) show a marked double-fibre texture. A clearer view of the texture is given by the ODF cuts shown in Figs. 6(*d*) and 6(*e*), where the main texture components are well represented. This double-fibre texture is similar to the one obtained for the HMS *Pomone* segment sample (Malamud *et al.*, 2016), with an intense γ-fibre with {111} planes parallel to the bolt axis and a minor ⟨100⟩ fibre component.

To define the full ODF for selected locations, neutron texture measurements were also performed in the sample to give an incomplete experimental pole figure for each of three other different positions across the bolt diameter (labelled B, C and D in Fig. 7). For each position the same experimental configuration and data analysis strategy was used as for the centre position (point A). For each location across the bolt diameter, the {111}, {200}, {220} and {311} experimental pole figures were generated from the integrated intensities and the respective correction factors for those virtual detectors with $\exp(-l\mu_{hkl}) > 0.01$. Fig. 7(*a*) shows the texture results, as the IPFs in the bolt axis direction, for each position across the sample cross section (using the same colour scale), together with the reference standard cubic crystallographic triangle. As is shown in the figure, the IPFs parallel to the bolt axis from all locations show the expected marked double-fibre texture. For point A the IPF presents a strong orientation of ⟨111⟩ along the BA, with a volume fraction of 43% of the crystallites, and a less intense orientation of the ⟨100⟩ poles along this sample direction, related to the minor ⟨100⟩ fibre component with a volume fraction of approximately 25% of the crystallites.

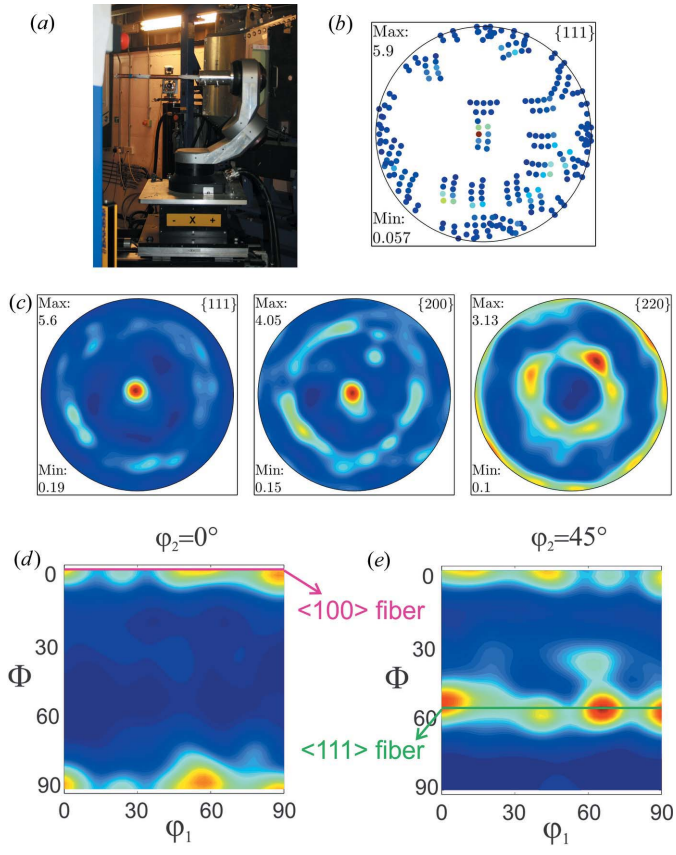

Figure 6
(*a*) Photograph of the HMS *Amethyst* sample in ENGIN-X. (*b*) Experimental pole figure showing the angular coverage achieved by the measurement. (*c*) Recalculated pole figures from the ODF, calculated with *MTEX* from experimental pole figures such as (*b*). (*d*), (*e*) Cuts of the ODF at $\varphi_2 = 0°$ and $\varphi_2 = 45°$, showing the main texture components of the material.

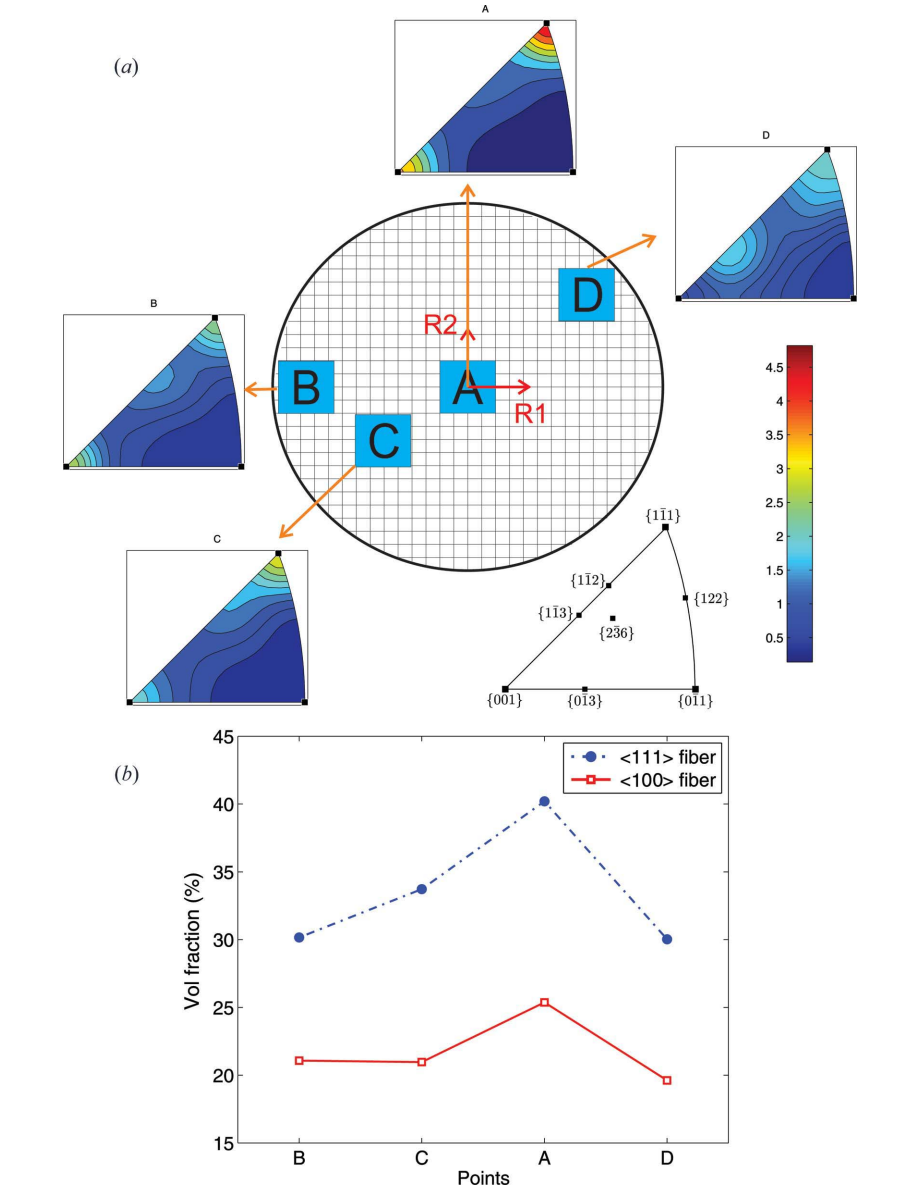

Figure 7
(*a*) Inverse pole figures from each measurement volume in the HMS *Amethyst* bolt (grid spacing 1 mm). All use the same colour scale in m.r.d. (*b*) ⟨111⟩ and ⟨100⟩ fibre component volume fractions for different locations across the HMS *Amethyst* bolt diameter.

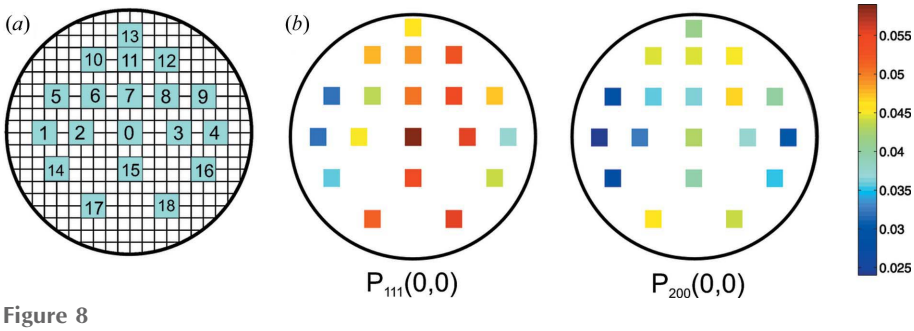

Figure 8
(*a*) Positions of the explored locations in the schematic cross section of the segment sample of the *Pomone* bolt (grid spacing 1 mm). (*b*) $P_{111}(0, 0)$ and $P_{200}(0, 0)$ pole figure intensities.

Fig. 7(*b*) shows the volume fraction of both fibre components for each location across the HMS *Amethyst* bolt diameter. As is shown in the figure, the ⟨111⟩ fibre texture volume fraction decreases from the centre to the surface of the bolt, while the ⟨100⟩ fibre maintains a volume fraction between 20 and 25% across the sample diameter. A similar double-fibre inhomogeneity has been reported in cold-drawn copper wires with high strains (Chen *et al.*, 2011) and could result from an inhomogeneous distribution of shear strain with radial position. This variation arose from the geometry of the deformation and from friction effects, leading to the shear strain increasing with increasing distance from the centres of the wires. This double-fibre deformation texture parallel to the drawing direction, as formed during a cold-drawing process, is completely consistent with the process patented by William Collins.

4.3. HMS *Pomone*

Two samples from HMS *Pomone* were studied, a complete bolt and a 'bolt segment', which was cut from a fragment (originally 33.5 mm in diameter) of a bolt from HMS *Pomone* that had previously been used for machining tensile test specimens. The complete bolt studied here (§4.3.2), find number AB1-02-01 in the excavation archive, is a blind bolt, 330 mm long and 22.5 mm in diameter, and was possibly used for fastening planking to a frame.

4.3.1. Bolt segment sample. The crystallographic texture at the centre of the copper bolt segment sample was determined using neutron diffraction and NyRTex data analysis, and the results were validated by complementary experiments using electron backscatter diffraction (EBSD) measurements and laboratory X-ray diffraction (Malamud *et al.*, 2016). In all cases, the recalculated pole figures for the segment showed a marked double-fibre texture: a strong γ-fibre with {111} planes parallel to the bolt axis and a minor ⟨100⟩ fibre component. This major component is one of the most common fibre textures, having the {111}

slip plane perpendicular to the direction of application of the force, while the presence of a ⟨100⟩ fibre texture reveals nearly complete thermal crystallization after working (Park & Lee, 2003). EBSD orientation images taken in the centre of a cross section through the bolt segment confirm the grain structure to be fully recrystallized, presenting moderate levels of deformation in the recrystallized grains.

As can be seen in Fig. 1(*c*), the diffractograms along the BA direction from different locations across the bolt segment's cross section suggested there to be a texture gradient across the bolt diameter. To investigate such variations, a series of neutron measurements were performed in the same orientations as Fig. 1(*a*) ($\chi = 90°$, $\omega = -45°$, $\varphi = 0°$), at several locations across the segment cross section. The experiments were performed using an incident beam divergence of ∼0.7 × 0.8° (horizontal × vertical) and a gauge volume of 2 × 2 × 2 mm centred at each position. The 19 explored locations are shown in Fig. 8 in a schematic cross section of the segment, together with the pole figure intensities in the bolt axis direction for the 111 and 200 reflections, $P_{111}(0, 0)$ and $P_{200}(0, 0)$, respectively. As is shown in the figure, the intensities $P_{111}(0, 0)$ generally decrease radially from the centre to the surface and in all locations they are higher than $P_{200}(0, 0)$. This double-fibre texture is typical of axi-symmetrically drawn products made of f.c.c. metals with medium or high stacking fault energies (Cho *et al.*, 2006).

To define the full ODF for selected locations, neutron texture measurements were performed on the segment sample to define incomplete experimental pole figures for the five locations across the segment diameter shown in Fig. 1(*b*). Point A is at the centre of the bolt and points B, C, D and E are centred at 7, −4, 4 and 7 mm from A, respectively. For each position, neutron experiments were performed using an incident beam divergence of ∼0.7 × 0.8° (horizontal × vertical) and a 4 × 4 × 4 mm gauge volume centred at each location. The bolt axis was placed horizontally ($\chi = 90°$), as shown in Fig. 1(*a*), and tilted to 45° from the vertical. For the tilted setup, four measurements were performed rotating the segment around the vertical instrument axis. In all the experimental configurations, TOF diffractograms were collected with counting times of ∼12 min per orientation. For each location across the segment diameter, the ODF was reconstructed from the experimental data using NyRTex. The data were analysed in a 2 × 5 (horizontal × vertical) gridding scheme, which gives each virtual detector a coverage of ∼8 × 8° in angular space. The {111}, {200}, {220} and {311} experimental pole figures were generated from the integrated intensities and the respective correction factors for those virtual detectors with $\exp(-l\mu_{hkl}) > 0.01$.

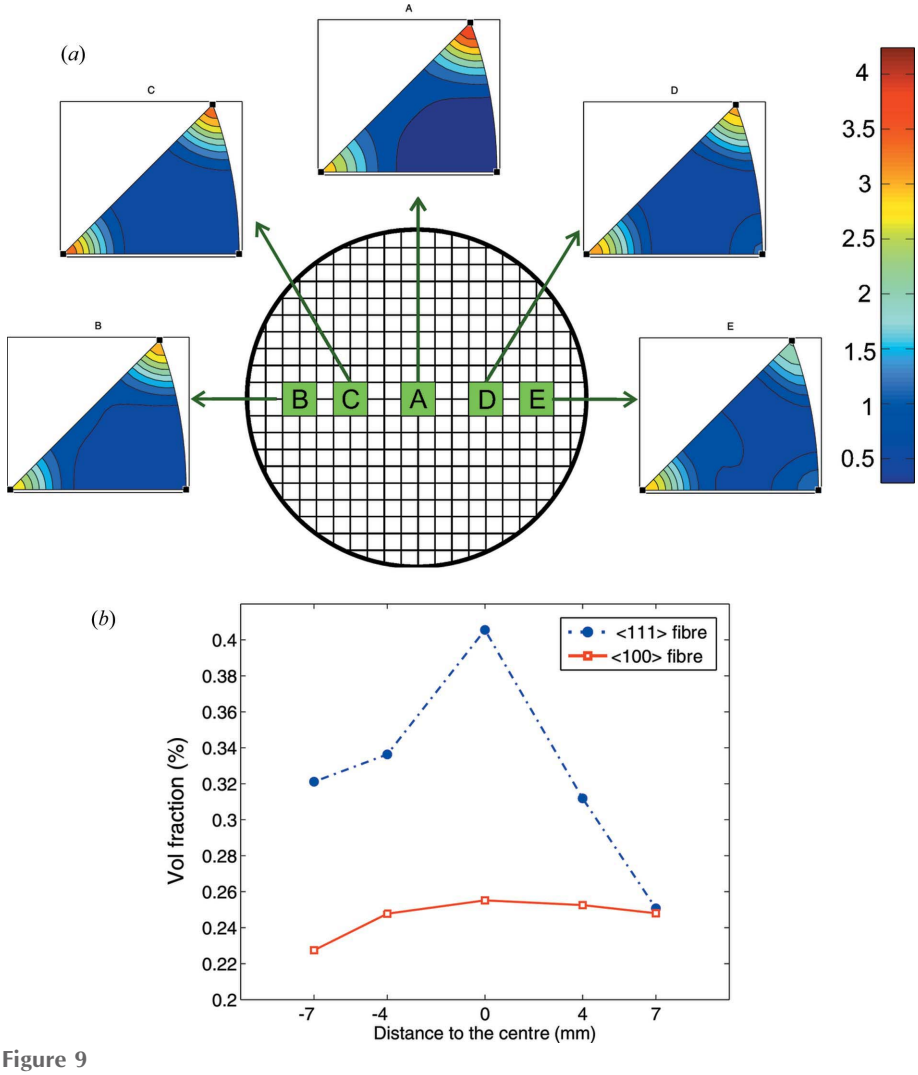

Figure 9
(*a*) The recalculated inverse pole figures along the bolt axis direction (BA) for each point across the *Pomone* bolt segment diameter (grid spacing 1 mm). (*b*) ⟨111⟩ and ⟨100⟩ fibre component volume fractions for different locations across the segment sample diameter.

The recalculated IPFs along the BA for each position across the bolt segment diameter are shown in Fig. 9(*a*), using the same colour scale, together with the reference standard cubic crystallographic triangle. The experimental IPFs relative to the bolt axis direction in all locations show the expected marked double-fibre texture. Notably, the IPF from position A shows a strong alignment of ⟨111⟩ along this specific direction, with values higher than 4 m.r.d. and a volume fraction of 40% of the crystallites giving an intense γ-fibre texture in the segment sample, and a less intense orientation of the 100 poles along the BA direction, related to the minor

⟨100⟩ fibre component with a volume fraction of approximately 25% of the crystallites.

Fig. 9(*b*) shows the volume fraction of each fibre component at locations across the segment diameter. As is shown in the figure, the ⟨111⟩ fibre texture volume fraction decreases from the centre to the surface of the bolt segment, while the ⟨100⟩ fibre volume fraction remains between 22 and 25% across the segment diameter. This behaviour is the same as that observed in the HMS *Amethyst* sample and is completely consistent with the process patented by William Collins.

4.3.2. AB1-02-01 sample. The central point texture of the AB1-02-01 sample was measured using an instrument configuration and data analysis strategy identical to that for the segment sample (Malamud *et al.*, 2016). The ODF of the material was calculated using NyRTex and *MTEX* from the {111}, {200}, {220} and {311} experimental pole figures assuming triclinic sample symmetry. The two main texture components are a $\{111\}\langle 1\bar{2}1\rangle$ component, with a volume fraction of 14% of the crystallites, and a {001}⟨100⟩ cube component, with a 15.5% volume fraction (volume fractions computed by *MTEX* using a 20° radius sphere centred at each orientation). The presence of the $\{111\}\langle 1\bar{2}1\rangle$ texture component indicates a good alignment of the {111} planes parallel to the BA, which is a feature commonly associated with extensional deformation along the symmetry axes of f.c.c. metallic wires (Artioli, 2007). On the other hand, the development of the high-symmetry {001}⟨100⟩ cube component is a direct manifestation of sample recrystallization. The similar volume fractions obtained for each component show the complete bolt to be only partially recrystallized. To study the variation of the volume fractions of each component across the bolt diameter, texture measurements were performed in different positions across the AB1-02-01 bolt cross section (Fig. 10*a*). The explored positions are schematically shown in Fig. 10(*c*), *i.e.* at the bolt centre (position A), close to the surface (positions B and C), and at intermediate positions (points D and E). As for the segment, a macroscopic coordinate system, centred at point A, was defined, by the BA and two perpendicular arbitrarily chosen radial directions R1 and R2.

These neutron experiments were performed using similar experimental configurations to those used in the bolt segment experiment [an incident beam divergence of ∼0.7 × 0.8° (horizontal × vertical) and rotating the sample using the Cybaman manipulator; Fig. 10(*a*)]. The bolt axis was placed vertically ($\chi = 0$ °), horizontally ($\chi = 90$ °), and tilted to 30 and 45° from the vertical, and several measurements were performed rotating the sample around the vertical instrument axis (varying ω) and around the bolt axis direction (varying φ). The experiments were performed using a 10 × 4 × 4 mm gauge volume in the vertical configuration, a 4 × 4 × 4 mm gauge in the horizontal configuration and a 6 × 4 × 4 mm gauge volume in the tilted cases. For each point in the HMS *Pomone* specimen cross section, the TOF diffractograms were recorded at 13 specimen orientations, with counting times of ∼12 min per orientation.

Similarly to in the segment experiment, the data were analysed in a 2 × 5 (horizontal × vertical) gridding scheme, which produces a total of 260 virtual detectors for the 13 orientations measured for each position. The {111}, {200}, {220} and {311} experimental pole figures were generated from the integrated intensities and the respective correction factors for those virtual detectors with $\exp(-l\mu_{hkl}) > 0.01$. This reduces the number of useful virtual detectors by about 15 or 20 for different reflections at each point. The pole figure coverage obtained for position A is shown in Fig. 10(*b*) as the {111} experimental pole figure. The ODF of the material was calculated with *MTEX* from the {111}, {200}, {220} and {311} experimental pole figures assuming triclinic sample symmetry, and the results for each point are shown in Fig. 10(*c*) as the recalculated IPFs looking along the BA. As seen in Fig. 11, for all points the principal features of the texture are similar to those obtained in the previous experiment, with intense {111} and {100} type components and smaller {011} and ∼{113} type components parallel to the bolt axis direction. In particular, a {001}⟨100⟩ cube component due

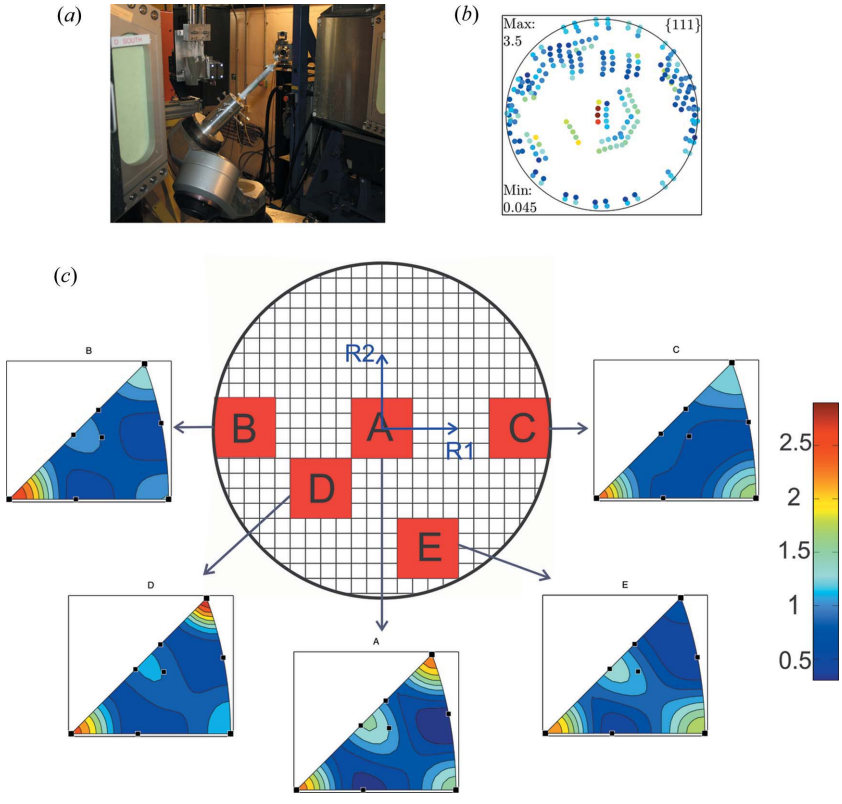

Figure 10
(*a*) Photograph of the *Pomone* bolt AB1-02-01 in ENGIN-X. (*b*) Position A {111} experimental pole figure. (*c*) Inverse pole figures from each measurement volume in the *Pomone* bolt (grid spacing 1 mm). All use the same colour scale in multiples of a random distribution.

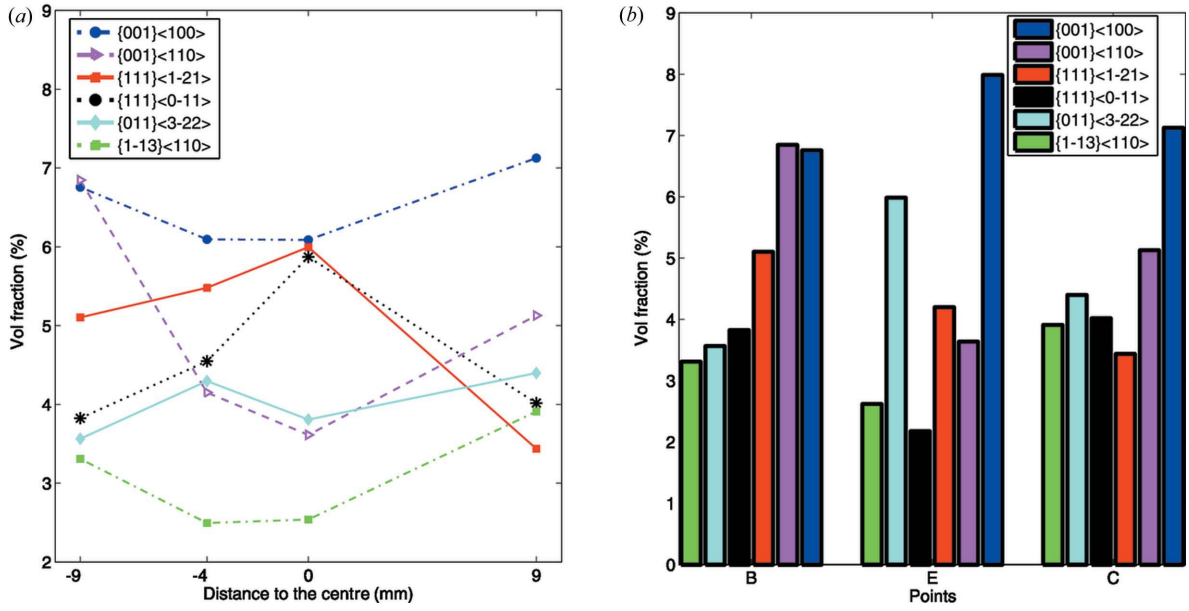

Figure 11
(*a*) Principal component volume fractions as a function of the distance from the bolt centre for the *Pomone* complete bolt. (*b*) Volume fractions for points close to the bolt surface.

to recrystallization and $\{111\}\langle 1\bar{2}1\rangle$ and $\{111\}\langle 0\bar{1}1\rangle$ components related to mechanical working were found in the BA direction. Those three texture components are all present in a similar volume fraction (∼6%, as computed by *MTEX* using a 15° radius sphere centred at each orientation) in the central point, as is shown in Fig. 11(*a*).

The volume fraction of the textural features related to mechanical working parallel to the BA decreases from the central point to the surface, while the recrystallization component increases. In particular, an extra recrystallization component, a $\{001\}\langle 320\rangle$ rotated cube component, emerges as one of the main texture components close to the surface, as is shown in Fig. 11(*b*) for the points close to the bolt surface (positions B, C and E). Regarding the less intense texture components, a slightly rotated brass component was identified, which can be described approximately as $\{011\}\langle 3\bar{2}2\rangle$, and a rotated Taylor component approximating to $\{1\bar{1}3\}\langle 110\rangle$. Both brass type and Taylor type texture components are typical deformation textures in f.c.c. materials (Kocks *et al.*, 2000), driven by the dominant slip system of the f.c.c. lattice $\{111\}\langle 110\rangle$.

4.4. HMS *Maeander*

Texture measurements were performed at two positions across the HMS *Maeander* bolt cross section: at the bolt centre (position A) and close to the surface (position B). The neutron experiments were performed using similar experimental configurations to those used in the other cases. The sample was rotated using the Cybaman manipulator and for each point the TOF diffractograms were recorded at ten specimen orientations, with counting times of ∼12 min per orientation, using a 4 × 4 × 4 mm gauge volume. The bolt axis was placed horizontally ($\chi = 90°$) and tilted to 45° from the vertical, and several measurements were performed rotating the sample around the vertical instrument axis (varying ω) and around the bolt axis direction (varying φ). The data were analysed in a 2 × 5 (horizontal × vertical) gridding scheme, which produces a total of 200 virtual detectors for the ten orientations measured for each position.

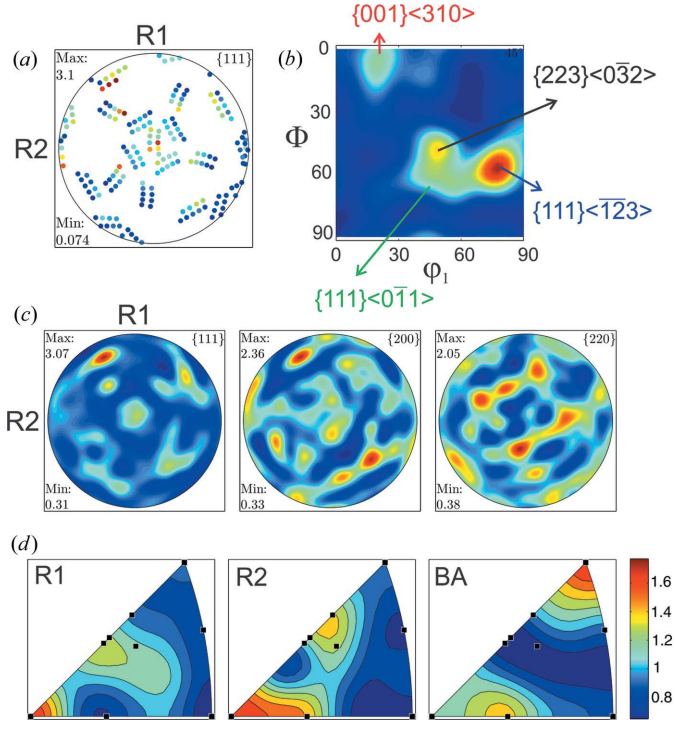

Figure 12
Maeander bolt: point A. (*a*) Experimental {111} pole figure. (*b*) $\varphi_2 = 45°$ ODF section. (*c*) Recalculated pole figures and (*d*) inverse pole figures.

Table 3
Principal texture components obtained for both explored positions across the HMS *Maeander* bolt.

Points	Texture component	Euler angles φ_1 (°)	Φ (°)	φ_2 (°)	Volume (%)
A	$\{111\}\langle 1\bar{2}3\rangle$	80	55	45	5.03
	$\{111\}\langle 0\bar{1}1\rangle$	60	55	45	4.18
	$\{223\}\langle 0\bar{3}2\rangle$	54	55	45	3.21
	$\{001\}\langle 310\rangle$	71.6	0	0	4.06
B	$\{112\}\langle \bar{1}\bar{1}1\rangle$	90	35	45	4.27
	$\{110\}\langle \bar{1}11\rangle$	35	90	45	6.38
	$\{001\}\langle 1\bar{5}0\rangle$	78	0	0	3.76

The {111}, {200}, {220} and {311} experimental pole figures were generated from the integrated intensities and the respective correction factors for those virtual detectors with $\exp(-l\mu_{hkl}) > 0.01$. The pole figure coverages obtained by this data analysis scheme for positions A and B are shown for the {111} experimental pole figures in Figs. 12(*a*) and 13(*a*), respectively. The ODF of the material was calculated with *MTEX* from the {111}, {200}, {220} and {311} experimental pole figures, assuming triclinic sample symmetry. The results for each point are shown in Fig. 12 for point A and Fig. 13 for point B. In both cases, the ODF is presented using the $\varphi_2 = 45°$ ODF cut (*b*) where the main texture components for each location are well represented. The recalculated pole figures are shown in (*c*) and the IPFs in the sample principal directions (R1, R2 and BA) in (*d*).

Figs. 12 and 13 suggest clearly different crystallographic textures at the two positions. The main texture components present in the ODF section plots are listed in Table 3, with their corresponding Euler angles (using the Bunge convention; Kocks *et al.*, 2000) and volume fractions (computed by *MTEX* using a 15° radius sphere centred at each orientation). For point A, the $\{111\}\langle 1\bar{2}3\rangle$, $\{111\}\langle 0\bar{1}1\rangle$ and $\{223\}\langle 0\bar{3}2\rangle$ components can be related to mechanical working in the bolt axis direction, and the ~$\{001\}\langle 310\rangle$ component is a rotated cube component, as results from recrystallization during thermal annealing of rolled f.c.c. metals. As is shown in Fig. 12(*d*), the IPF in the BA direction shows a strong alignment of the $\langle 111\rangle$ poles along this specific direction, with the $\langle 100\rangle$ poles orientated along the perpendicular directions R1 and R2. On the other hand, for point B the principal texture components are $\{001\}\langle 1\bar{5}0\rangle$, $\{112\}\langle \bar{1}\bar{1}1\rangle$ and $\{110\}\langle \bar{1}11\rangle$, as is shown in the ODF section (Fig. 13*b*). In this case, as is shown in the IPFs, there is a strong alignment of the $\langle 111\rangle$ poles in the R1 and R2 directions. This behaviour could be associated with a strong mechanical working perpendicular to the bolt axis direction, probably relating to a hammering process after the heat treatment.

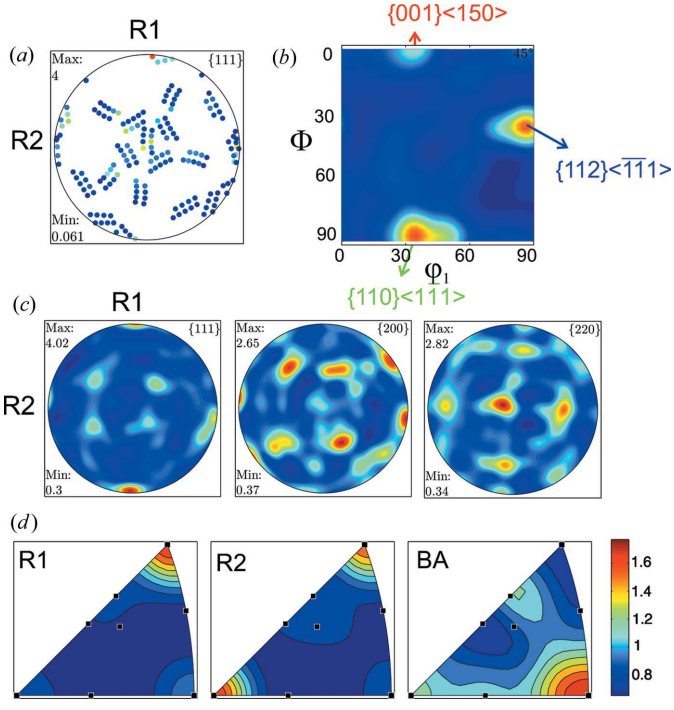

Figure 13
Maeander bolt: point B. (*a*) Experimental {111} pole figure. (*b*) $\varphi_2 = 45°$ ODF section. (*c*) Recalculated pole figures and (*d*) inverse pole figures.

5. Discussion

In this work we have employed a new texture analysis methodology using ENGIN-X, a TOF neutron strain scanner, to perform nondestructive texture analyses to study texture gradients across cross sections of copper bolts. In particular, we have analysed four copper bolts from the wrecks of HMS *Impregnable* (completed 1786), HMS *Amethyst* (1799), HMS *Pomone* (1805) and HMS *Maeander* (1840) along with a cylindrical 'segment' of a further incomplete bolt from HMS *Pomone*. Previous measurements (Malamud *et al.*, 2016) have identified three distinctly different types of texture in British naval bolts from a similar period, two of which can definitely be identified with the Collins and Forbes processes and a third which may have resulted from the Westwood process.

The bolt with a Forbes stamp from HMS *Impregnable* came from the lower part of the hull and can probably be dated to her conversion to copper bolts, which started late in 1783 when William Forbes received his order for them. The bolt had a relatively weak texture, indicating a recrystallized microstructure, retaining some features relating to working in the bolt axis direction. There was a pronounced variation in the texture across the cross section: the centre of the bolt still shows the effects of axial deformation, whereas the cube texture characteristic of recrystallization predominates close to the edges of the bolt.

Besides the outline of Forbes's process in the specification for his 1783 patent, there are also records describing day to day operations in his rolling mill in relation to heat treatment and cold hardening of the exterior shell of the bolt using a tilt hammer and swage on the 'larger' bolts. The mill produced bolts up to 54 mm in diameter and there is no clue from documentation what size range of bolts received further cold hardening. The texture of this 35.5 mm diameter bolt is completely consistent with the patented process and shows no evidence of cold working of the surface so we can infer that

Table 4
Summary of the major results.

Ship	Date completed	Sample type	Stamp	Diameter (mm)	Texture components: Central	Texture components: Rim	Deduction	Historical notes on use of Cu bolts
HMS *Impregnable*	1786	Bolt IMP-006	Forbes	35.5	{001}⟨100⟩ {122}⟨212⟩ {111}⟨2$\bar{3}$1⟩ {111}⟨$\bar{1}\bar{1}$2⟩	As centre but more {001}⟨100⟩ (+ {112}⟨$\bar{1}\bar{1}$1⟩ and {4 4 11}⟨11 $\bar{1}$1 $\bar{8}$⟩) and less {$\bar{1}\bar{1}$1}⟨2$\bar{3}$1⟩ and {111}⟨$\bar{1}\bar{1}$2⟩.	Partial recrystallization during annealing after rolling along the bolt axis direction: more {001}⟨100⟩ close to surface owing to recrystallization. Shear components close to surface may be due to documented cold hardening, driving or stresses of ship breakup.	Early in their general application.
HMS *Amethyst*	1799	Bolt	Westwood and Collins	41	Double fibre texture: major component {111} planes parallel to the bolt axis + minor ⟨100⟩ fibre component.	⟨111⟩ fibre fraction decreases from the centre to the surface of the bolt while ⟨100⟩ fibre fraction roughly constant.	While stamped Westwood and Collins, drawn texture completely consistent with the Collins process.	Early in their general application.
HMS *Pomone*	1805	Bolt AB1-02-01	None	22.5	{111}⟨1$\bar{2}$1⟩ {001}⟨100⟩	The volume fraction of the textural features related to mechanical working parallel to the bolt axis decreases from the central point to the surface, while the recrystallization component increases.	Extensional deformation along bolt length + partial recrystallization. Consistent with the Collins process.	Mature production in private mills.
		Segment	None	Originally 33.5	Double-fibre texture: major component {111} planes parallel to the bolt axis + minor ⟨100⟩ fibre component.	⟨111⟩ fibre fraction decreases from centre to surface, while the ⟨100⟩ fibre fraction remains constant.	Drawn texture completely consistent with the Collins process.	Mature production in private mills.
HMS *Maeander*	1840	Bolt	None	35.5	{111}⟨$\bar{1}\bar{2}$3⟩ {111}⟨0$\bar{1}$1⟩ {223}⟨0$\bar{3}$2⟩ {001}⟨310⟩	{001}⟨1$\bar{5}$0⟩ {112}⟨$\bar{1}\bar{1}$1⟩ {110}⟨$\bar{1}$11⟩ with strong alignment of ⟨111⟩ in two perpendicular radial directions.	Central texture shows probable rolling and thermal annealing. Absence of torsional components near surface suggests the ⟨111⟩ alignment is due to hammering.	Production only at Portsmouth dockyard.

bolts of this size or smaller were produced using the patented process without further treatment.

There was less variation across the cross section of the long bolt from HMS *Amethyst* (completed 1799) stamped 'Westwood Collins'. Although the texture was slightly stronger towards the centre, throughout the cross section there was a pronounced double-fibre texture, the major component being ⟨111⟩ along the bolt axis and the minor one ⟨100⟩ along the same direction. This is very close to that already determined (Malamud *et al.*, 2016) for the central segment of a bolt from the *Pomone* and definitely identifies the bolt as having been made by the Collins process of drawing the bolt through a die. At an earlier stage in this research it was suggested that the smallest-diameter bolts were the ones most likely to be drawn using Collins's process, but the *Amethyst* results show that noticeably larger bolts could also be drawn. From this we can begin to calculate the power output of the waterwheel driving the mill and relate it to the geography of the works used by Westwood and Collins in Greenfield, Holywell, in north-east Wales.

The segment of a large bolt from the *Pomone* (completed 1805) again showed a strong double-fibre texture with a stronger ⟨111⟩ and a weaker ⟨100⟩ component along the bolt axis. The ⟨111⟩ volume fraction decreased from the centre to the surface of the bolt, while the ⟨100⟩ alignment is similar all the way through. As for the bolt from the *Amethyst*, this is completely consistent with the Collins process.

At the centre of the bolt AB1-02-01 (330 mm long and of 22.5 mm diameter) from the *Pomone* there were similar volume fractions of the {111}⟨1$\bar{2}$1⟩ component related to extension along the bolt axis and the {001}⟨100⟩ cube component typical of recrystallization. There was also a

{111}⟨0$\bar{1}$1⟩ component related to extension along the bolt axis. The proportions of both the components relating to axial extension and other components relating to mechanical working reduced from the centre to the edge, while extra components, relating to recrystallization, were visible close to the bolt edge. There are still challenges in interpreting these results because the documents suggest a variable amount of swaging in finishing the bolts, but the texture shows no immediate evidence of such working.

The texture of the *Maeander* (laid down 1829 and launched 1840) bolt was very different from the textures of the others. As in the other bolts, there were differences in texture between the centre and close to the surface. Although the central texture again showed both components related to mechanical working along the BA and others related to recrystallization, there is no simple double-fibre texture. The differences were even more marked close to the surface where there was a strong alignment of ⟨111⟩ along one particular radial direction with a weaker alignment along the radius perpendicular to this. This intense directional mechanical working along particular radial directions close to the surface suggests that there may have been substantial hammering of the surface of the bolt. Any mechanical work in a radial direction might have produced an alignment of ⟨111⟩ along that direction, but groove-rolling or flexion during service should also have produced some torsion texture and there was no evidence of such texture components close to the surface. This is rather surprising given that the bolt was almost certainly produced at the Metal Mill in Portsmouth Dockyard which by 1829 already had over 20 years of experience and would be expected to have refined their processes to eliminate the need for hand finishing. The texture results could point to reshaping and reuse of a bolt from a vessel being scrapped, but we could simply be overestimating the capabilities of the Metal Mill. A summary of the major results in this paper and the deductions made from them is given in Table 4

The virtual cross sections of the bolts provided by spatially resolved texture analysis using neutron diffraction provides data about the manufacture, properties and use of copper bolts used by the Royal Navy from the end of the American War of Independence to beyond the end of the Napoleonic Wars. To minimize the impact on such cultural heritage objects, the maximum sample volume whose removal would be permitted for metallographic examination is of the same order as the gauge volumes used in these experiments, and so metallography could provide only a fraction of the information. Where the taking of cross sections is allowed they tend to be from damaged and fractured bolts where the as-manufactured texture may have been modified.

The next stage in this research is to pursue further the relationship between the textures, the observed microstructure and the bolts' mechanical properties. A recent hardness map made on a cross section of a bolt from HMS *Trincomalee*, a sister ship of *Pomone* and *Amethyst*, shows that the typical hardness values are quite low (Vickers hardness of 100–110) and variations in hardness do not clearly correspond to changes in texture and microstructure. Available cross sections, at least one of which is from a Collins bolt, will be used to compare and correlate local texture (by EBSD), microstructure and hardness to further illuminate the neutron diffraction data. To support the interpretation of the texture results, it is also possible to consider complementary information on micro-strain effects. However, measuring micro-strain across the bolt section using peak broadening analysis of the neutron diffraction profiles would require a different experimental setup. Another approach will be to look at the surface condition of bolts. The bolt from the *Amethyst* that was made by the Collins process showed parallel longitudinal striations in its surface which are reminiscent of those seen under a microscope on drawn wire. If further bolts with this appearance are identified and prove to have the same fibre texture we will have a rapid means of sorting bolts of that type, based on surface appearance, even when, as is usually the case, they are lacking the supposedly mandatory maker's stamps.

6. Conclusions

Using the new texture analysis methodology NyRTex and the TOF neutron strain scanner ENGIN-X, the texture and texture gradients in four copper bolts from Royal Navy ships completed between 1786 and 1840 have been determined nondestructively. Previous measurements (Malamud *et al.*, 2016) had identified three distinctly different types of texture in British naval bolts from a similar period, two of which can definitely be identified with the Collins and Forbes processes and a third which may have resulted from the Westwood process.

The principal conclusions from this study are as follows:

(1) The texture of the 35.5 mm diameter bolt with a Forbes stamp, manufactured in the early years of the general application of copper bolts, is completely consistent with Forbes's patented process. The variation in texture across the cross section reflects increased recrystallization approaching the surface and shows no evidence of any cold working of the surface, described in Forbes's mill records as having been used on 'larger' bolts, indicating that bolts of this size or smaller were produced using the patented process without further treatment.

(2) The double-fibre texture throughout the 41 mm diameter long bolt from HMS *Amethyst* stamped 'Westwood Collins' (again manufactured in the early years of copper bolts' general application) identifies the bolt as having been made by the Collins process of drawing the bolt through a die. This shows that the use of this process was not limited to smaller bolts. Modelling the power output required of the waterwheel driving the mill to draw a bolt of this diameter, as specified in the patent, would allow determination of the minimum river flow that would allow year-round working of the mill used by Westwood and Collins.

(3) Although the patent documents suggest a variable amount of swaging in finishing the bolts, the textures of the bolts from the *Pomone* (representative of the mature phase of copper bolt production in private mills) are consistent with the Collins process and show no immediate evidence of such

working. In the segment from a large bolt the ⟨111⟩ volume fraction decreased from the centre to the surface of the bolt while the ⟨100⟩ alignment was similar all the way through. In the 22.5 mm diameter bolt the proportions of the texture components relating to axial extension and mechanical working reduced from the centre to the edge while close to the bolt edge there were extra components relating to recrystallization.

(4) The texture of the bolt from the *Maeander*, later in the application of copper bolts, was very different from the textures of the others and suggests that there may have been substantial hammering of the surface of the bolt. The central texture showed both components related to mechanical working along the bolt axis and others related to recrystallization, but there was no simple double-fibre texture. Close to the surface there was a strong alignment of ⟨111⟩ along one particular radial direction with a weaker alignment along the radius perpendicular to this. The bolt was almost certainly produced at the Metal Mill in Portsmouth Dockyard which by 1829 already had over 20 years of experience and would be expected to have refined their processes to eliminate the need for hand finishing. The texture could point to reshaping and reuse of a bolt from a vessel being scrapped or it might be that process control at the Metal Mill was still fallible.

(5) Parallel longitudinal striations, as seen on the surface of the bolt from the *Amethyst*, may be diagnostic of a bolt made by the Collins process

As more dated shipwreck material becomes available, further texture analysis by neutron diffraction will provide information to let us explore in more detail the evolution of a significant technology.

References

Arletti, R., Cartechini, L., Rinaldi, R., Giovannini, S., Kockelmann, W. & Cardarelli, A. (2008). *Appl. Phys. A*, **90**, 9–14.

Artioli, G. (2007). *Appl. Phys. A*, **89**, 899–908.

Artioli, G. & Dugnani, M. (2004). *Period. Mineral.* **73**, 5–16.

Bunge, H. J. (1982). *Texture Analysis in Materials Science: Mathematical Methods*. London: Butterworths.

Cartechini, L., Rinaldi, R., Kockelmann, W., Bonamore, S., Manconi, D., Borgia, I., Rocchi, P., Brunetti, B. & Sgamellotti, A. (2006). *Appl. Phys. A*, **83**, 631–636.

Chen, J., Yan, W., Li, W., Miao, J. & Fan, X. (2011). *Trans. Nonferrous Met. Soc. China*, **21**, 152–158.

Cho, J.-H., Rollett, A. D., Cho, J.-S., Park, Y.-J., Park, S.-H. & Oh, K. H. (2006). *Mater. Sci. Eng. A*, **432**, 202–215.

Forbes, D. (1783). *Letters from David Forbes to William Forbes, October–December 1783*. Falkirk Archives A727.1766/1-4.

Forbes, W. (1783). UK Patent Specification No. 1381.

Hielscher, R. & Schaeben, H. (2008). *J. Appl. Cryst.* **41**, 1024–1037.

Imberti, S., Kockelmann, W., Celli, M., Grazzi, F., Zoppi, M., Botti, A., Sodo, A., Imperiale, M. L., de Vries-Melein, M., Visser, D. & Postma, H. (2008). *Meas. Sci. Technol.* **19**, 034003.

James, J., Santisteban, J., Edwards, L. & Daymond, M. (2004). *Phys. B Condens. Matter*, **350**, E743–E746.

Kockelmann, W., Chapon, L. C., Engels, R., Schelten, J., Neelmeijer, C., Walcha, H.-M., Artioli, G., Shalev, S., Perelli-Cippo, E., Tardocchi, M., Gorini, G. & Radaelli, P. G. (2006). *J. Neutron Res.* **14**, 37–42.

Kockelmann, W. & Kirfel, A. (2004). *Phys. B Condens. Matter*, **350**, E581–E585.

Kockelmann, W., Kirfel, A. & Hähnel, E. (2001). *J. Archaeol. Sci.* **28**, 213–222.

Kockelmann, W., Siano, S., Bartoli, L., Visser, D., Hallebeek, P., Traum, R., Linke, R., Schreiner, M. & Kirfel, A. (2006). *Appl. Phys. A*, **83**, 175–182.

Kocks, U. F., Tome, C. N. & Wenk, H.-R. (2000). *Texture and Anisotropy: Preferred Orientations in Polycrystals and Their Effect on Materials Properties*. Cambridge University Press.

Kropff, F., Granada, J. R. & Mayer, R. E. (1982). *Nucl. Instrum. Methods Phys. Res.* **198**, 515–521.

Langh, R. van, Bartoli, L., Santisteban, J. & Visser, D. (2011). *J. Anal. At. Spectrom.* **26**, 892–898.

Malamud, F., Northover, S., James, J., Northover, P. & Kelleher, J. (2016). *Appl. Phys. A*, **122**, 276.

Malamud, F., Santisteban, J. R., Vicente Alvarez, M. A., Bolmaro, R., Kelleher, J., Kabra, S. & Kockelmann, W. (2014). *J. Appl. Cryst.* **47**, 1337–1354.

Matthies, S., Pehl, J., Wenk, H.-R., Lutterotti, L. & Vogel, S. C. (2005). *J. Appl. Cryst.* **38**, 462–475.

Nneji, S. O., Zhang, S. Y., Kabra, S., Moat, R. J. & James, J. A. (2016). *Nucl. Instrum. Methods Phys. Res. Sect. A*, **813**, 123–131.

Northover, J. P. (2007). *When Archaeometry and Conservation Meet*, Metal07, Vol. 1, ICOM Conference Preprint, edited by C. Degrigny, pp. 83–90. Amsterdam: Rijksmuseum.

Northover, J. P., Northover, S. M., James, J. & Malamud, F. (2014). *The Maritime Archaeology of Alum Bay. Two Shipwrecks on the Northwest Coast of the Isle of Wight, England*, British Archaeological Reports, British Series 608, edited by J. Satchell & J. Whitewright, pp. 48–55. Oxford: Archaopress.

Northover, J. P. & Wilcox, N. (2013). *Matthew Boulton: Enterprising Industrialist of the Enlightenment*, edited by K. Quickenden, S. Baggott & M. Dick, pp. 101–110. Farnham: Ashgate Publishing Ltd.

Park, H. & Lee, D. N. (2003). *Metall. Mater. Trans. A*, **34**, 531–541.

Randle, V. & Engler, O. (2000). *Introduction to Texture Analysis: Macrotexture, Microtexture & Orientation Mapping*. Amsterdam: Gordon & Breach.

Santisteban, J. R., Daymond, M. R., James, J. A. & Edwards, L. (2006). *J. Appl. Cryst.* **39**, 812–825.

Santisteban, J. R., Siano, S. & Daymond, M. R. (2006). *Mater. Sci. Forum*, **524–525**, 975–980.

Siano, S., Bartoli, L., Kockelmann, W., Zoppi, M. & Miccio, M. (2004). *Phys. B Condens. Matter*, **350**, 123–126.

Siano, S., Bartoli, L., Santisteban, J. R., Kockelmann, W., Daymond, M. R., Miccio, M. & De Marinis, G. (2006). *Archaeometry*, **48**, 77–96.

Taylor, A. (1961). *X-ray Metallography*. New York: Wiley.

Wang, D.-Q., Santisteban, J. R. & Edwards, L. (2001). *Nucl. Instrum. Methods Phys. Res. Sect. A*, **460**, 381–390.

Williams, W. G., Ibberson, R. M., Day, P. & Enderby, J. E. (1997). *Phys. B Condens. Matter*, **241–243**, 234–236.

Xie, Y., Lutterotti, L., Wenk, H. R. & Kovacs, F. (2004). *J. Mater. Sci.* **39**, 3329–3337.